POLARIMETRIC RADAR ANALYSIS OF POTENTIALLY ICE-HOSTING PSRS FROM MERCURY TO THE MOON. E. G. Rivera-Valentín[1], S. S. Bhiravarasu[2], A. K. Virkki[3], M. C. Nolan[4], T. P. Himani[5], G. W. Patterson[1], H. M. Meyer[1], N. L. Chabot[1]; [1]Johns Hopkins University Applied Physics Laboratory, [2]Space Applications Centre, Indian Space Research Organization, [3]Univ. of Helsinki, [4]Lunar and Planetary Laboratory, Univ. of Arizona, [5]Dept. of Earth and Planetary Science, Johns Hopkins University.

Introduction: Ground-based radar observations readily identified volatile deposits within permanently shadowed regions (PSRs) of some polar Mercurian craters due to their high backscatter and circular polarization ratio (CPR) [1,2]. Such properties are similar to those of the icy Galilean moons and the Martian polar ice deposits [3,4], suggesting regions of nearly-pure water ice [5]. Indeed, later observations by MESSENGER provided support for this interpretation [e.g., 6].

Although the thermal environment of lunar PSRs also allows for stable water ice [7], they do not exhibit enhanced backscatter and CPR in Arecibo S- (12.6 cm, 2380 MHz) or P-band (70 cm, 430 MHz) radar imagery [8,9]. Yet, using spectra from the Moon Mineralogy Mapper, [10] found evidence of exposed surficial water ice within some lunar PSRs. Furthermore, using the Miniature Radio Frequency (Mini-RF) instrument aboard the Lunar Reconnaissance Orbiter (LRO), [11] found that bistatic S-band measurements of Cabeus crater showed an opposition effect potentially indicative of buried ice. Dielectric permittivity inversion studies using radar measurements with Mini-RF and the Dual Frequency Synthetic Aperture Radar (DFSAR) aboard Chandrayaan-2 have also identified locations of high dielectric permittivity within some lunar PSRs [12,13]. However, the studied craters all have CPR < 1, which is not expected for multiple scattering events within ice where $1 \lesssim \mathrm{CPR} \lesssim 2$ is predicted [14]. Thus, CPR may not be a robust diagnostic tool to identify volatile deposits. Indeed, [15] showed that the CPR of the radar bright features at the north pole of Mercury are indistinguishable from the background, non-icy regolith.

Recently, [16] proposed a new polarimetric analytical technique to investigate radar scattering. In their work, [16] proposed that the same-circular (SC) and opposite-circular (OC) backscatter coefficients can be used separately to improve target characterization. Here, we leverage this technique to revisit the northern Mercurian polar deposits and some lunar PSRs.

Mercury: We used the Arecibo S-band radar observations collected during the 2019 inferior conjunction presented in [15]. In their work, they showed that variation in the radar backscatter of the north polar PSRs can be attributed to differences in ice purity. Additionally, by using a *k*-means clustering algorithm, they found that while some craters show a central bright feature surrounded by lower backscatter in a gradational pattern, other craters presented a mottled radar return.

Here we studied the radar scattering properties of PSRs within five large craters at Mercury's north pole – Chesterton, Tolkien, Tryggvadóttir, Kandinsky, and Prokofiev – to further investigate the two observed patterns. Of these craters, Chesterton, Tolkien, and Tryggvadóttir presented a gradational pattern in their backscatter while Kandinsky and Prokofiev did not. The SC and OC backscatter coefficients for the highest and lowest *k*-means classes were sampled and, following [16], we did a linear least-squares fit (LSF) to the measurements. In their work, [16] showed that the LSF slope describes the abundance and morphology of wavelength-scale scatterers and the intercept the dielectric permittivity. In Fig. 1, we show the LSF derived values ratioed with the background, non-icy terrain.

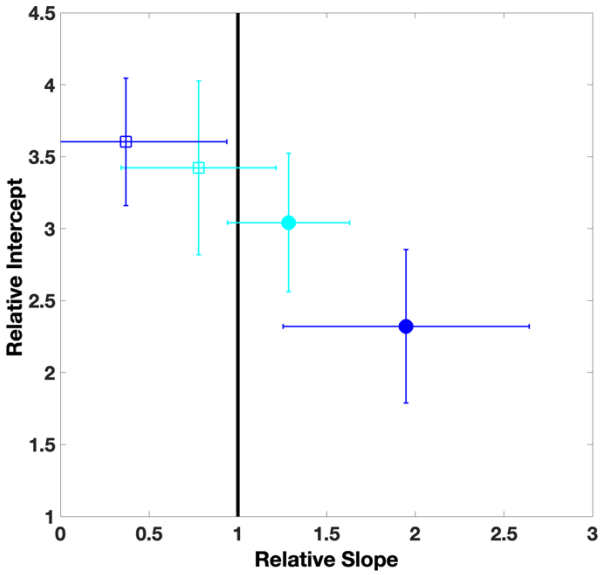

Figure 1: LSF slope and intercept relative to the background non-icy terrain for Chesterton, Tolkien, and Tryggvadóttir (circles), and Kandinsky and Prokofiev (squares) for the highest (cyan) and lowest (blue) SC radar backscatter (i.e., high and low *k*-means classes from [15]). Error bars are 2-σ.

Regardless of backscatter intensity, all craters exhibit a LSF intercept higher than the background terrain, suggesting their dielectric permittivity is higher. The brightest regions within Kandinsky and Prokofiev result in an intercept that is indistinguishable from that obtained using the lowest backscatter. This suggests that brightness variations within craters with a mottled radar return are likely not dominated by differences in dielectric permittivity. On the other hand, the highest

backscatter from craters exhibiting a gradational pattern results in an intercept that is higher than the lowest backscatter. This suggests that radar bright regions within Chesterton, Tolkien, and Tryggvadóttir likely have a higher dielectric permittivity than less bright regions, in agreement with [15]. The brightest regions within the studied craters also result in a slope that is not fully distinguishable from the background, non-icy terrain. This may indicate similarities in the wavelength-scale scatterers. Interestingly, lower backscatter regions within Chesterton, Tolkien, and Tryggvadóttir have a higher LSF slope than the background terrain, indicating a material dominated by less and/or smoother scatterers, while similar regions within Prokofiev and Kandinsky have a lower slope. This suggests further local-scale complexities in the Mercurian deposits.

The Moon: For this study, we chose PSR-hosting lunar craters with radar signatures indicative of ice [11-13]: Cabeus, both an unnamed crater within it (85.5°S, 308.2°E) and the large PSR near a crater wall (84.4°S, 314.1°E), Hermite, both the large PSR (84.8°N, 251.9°E) and an unnamed small crater within it (87.1°N, 273.7°E), Hermite A (87.9°N, 309°E), and Malinkin (87.2°S, 75.9°E). We used Mini-RF monostatic radar products, which include maps of the four Stokes parameters, to derive the SC and OC backscatter. The radar backscatter coefficients were then sampled from controlled polar mosaics of the north and south pole. The derived LSF slopes and intercepts of the PSR locations were ratioed against non-PSR regions within or near the same crater and within the same Mini-RF collect. The results are shown in Fig. 2.

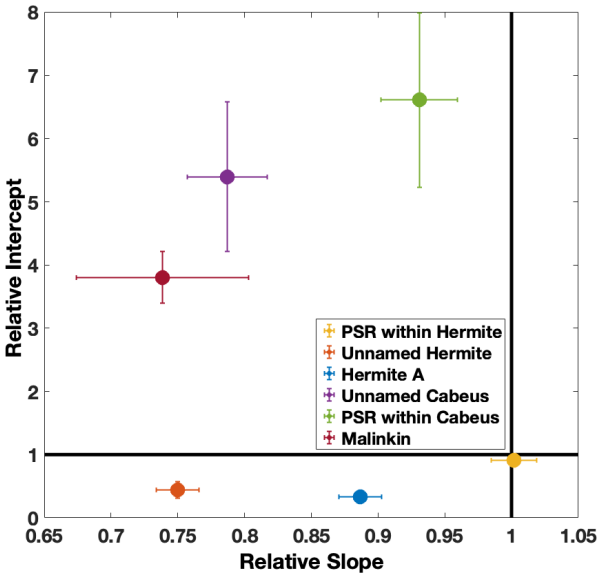

Figure 2: The LSF slope and intercept relative to non-PSR terrain for the studied lunar craters (circles) following the color code in the legend. Error bars are 2-σ.

The backscatter from the studied PSRs within Cabeaus and Malinkin result in an intercept that is higher than non-PSR terrain. This would suggest these areas have a higher dielectric permittivity than ice-free regolith, which could be due to slabs of ice or, more generally, a higher bulk density. On the other hand, the unnamed crater within Hermite and Hermite A both have backscatter that results in a lower intercept. This is indicative of a material with a lower dielectric permittivity, which could be due to lower bulk density, as in a substrate composed of ice, rock, and significant porosity. These craters also are all characterized by a lower slope than non-PSR terrain, which would imply more and/or rougher scatterers. Finally, the derived LSF intercept and slope for the large PSR within Hermite crater are indistinguishable from ice-free regolith. As such, it likely hosts little to no ice.

Conclusions: The polarimetric analytical technique from [16] reproduces radar modeling results from [15] and improves characterization of the Mercurian north polar ice deposits. Indeed, we identified additional local-scale heterogeneities between Mercurian PSRs. For the Moon, we found that the large PSR within Hermite crater likely hosts little to no ice, unlike suggested by [12]. We also identified variations in the dielectric permittivity of regolith within PSRs, which is supportive of dielectric inversion studies [13] and may point to locations of ice deposits, as suggested by the observed opposition effect with Mini-RF bistatic data [11]. We found that, unlike on Mercury, some lunar PSRs have a lower dielectric permittivity than non-icy regions, indicating patchy and/or porous ice. Thus, such ice deposits on the Moon may be older and/or more processed than Mercurian deposits, as suggested by [17].

Acknowledgements: This work was supported by NASA through LRO's Mini-RF instrument. Controlled polar mosaics of Mini-RF data were produced by R. Kirk (USGS). The Arecibo planetary radar project is funded by NASA.

References: [1] Harmon, J. K. & Slade, M. A. (1992) Science 258, 640-643. [2] Slade, M. A. et al. (1992) Science 258, 635-640. [3] Ostro, S. J. et al. (1992) JGR 97, 18227-18244. [4] Muhleman, D. O. et al. (1991) Science 253, 1508-1513. [5] Butler, B. J. et al. (1993) JGR 98, 15003-15023. [6] Lawrence, D. J. et al. (2013) Science 339, 292-296. [7] Vasavada, A. R. et al. (1999) Icarus 141, 179-193. [8] Stacey, N. J. S. et al. (1997) Science 276, 1527-1530. [9] Campbell, B. A. et al. (2003) Nature 426, 137-138. [10] Li, S. et al. (2018) PNAS 115, 8907-8912. [11] Patterson, G. W. et al. (2017) Icarus 283, 2-19. [12] Singh, A. et al. (2022) Adv. in Space Research 70, 4030-4055. [13] Sharma, A. et al. (2023) Icarus 391, 115350. [14] Hapke, B. (1990) Icarus 88, 407-417. [15] Rivera-Valentín, E. G. et al. (2022) PSJ 3, 62. [16] Virkki, A. K. and Bhiravarasu, S. S. (2019) JGRP 124, 3025-3040. [17] Costello, E. S. et al. (2020) JGRP 125, e2019jE006172.